Criteria for and statistics of electron diffusion regions associated with subsolar magnetic field reconnection

F. S. Mozer

Physics Department and Space Sciences Laboratory, University of California, Berkeley, Berkeley, California, USA

Received 8 June 2005; revised 4 October 2005; accepted 19 October 2005; published 28 December 2005.

[1] The definition of "electron diffusion regions" and criteria for identifying them in magnetic field reconnection events are given. By employing these criteria and further constraints on the measured parallel electric field, 117 electron diffusion regions have been found in searching through 3 years of Polar satellite subsolar data. They exist in filamentary currents in which parallel electric fields and depressed plasma densities are found and where the electron beta is generally less than 1. The average parallel electric field in these events is about 30% of the average 38 mV/m perpendicular field. The size of these regions is the order of the electron skin depth or less. These electron diffusion regions are topological boundaries in the electron and magnetic field line flows because the components of $\mathbf{E} \times \mathbf{B}/B^2$ on their opposite sides are frequently different. These regions are found throughout the magnetopause but mainly at the magnetospheric separatrix. The divergence of the pressure tensor in the Generalized Ohm's Law may be the leading term that balances the parallel electric field if the observed large plasma density variations (and hence electron pressure variations) were spatial and not temporal. The picture resulting from this data is of a magnetopause that is highly structured and filamentary and very different from a linear, laminar, symmetric structure sometimes considered in theories or simulations. However, it is emphasized that events such as those described have been found in fewer than 20% of the magnetopauses examined, so the conventional picture may be more prevalent.

Citation: Mozer, F. S. (2005), Criteria for and statistics of electron diffusion regions associated with subsolar magnetic field reconnection, *J. Geophys. Res.*, *110*, A12222, doi:10.1029/2005JA011258.

1. Introduction

[2] By subtraction of Newton's Second Law for an electron fluid from that for an ion fluid and after some approximations, the Generalized Ohm's Law is obtained as [*Spitzer*, 1956]

$$\mathbf{E} + \mathbf{U_I} \times \mathbf{B} = c\mathbf{j} \times \mathbf{B}/en - c\nabla \cdot \mathbf{P}_e/en + (m_e c^2/ne^2)\delta\mathbf{j}/\delta t + \eta\mathbf{j}, \quad (1)$$

where $\mathbf{E}$ and $\mathbf{B}$ are the electric and magnetic fields, $\mathbf{U}_I$ is the velocity of an element of ion fluid, $\mathbf{j}$ and n are the current and plasma densities, respectively, η is the resistivity associated with ion-electron interactions, and $\nabla \cdot \mathbf{P}_e$ is the divergence of the electron pressure tensor. Equivalently, by writing $\mathbf{j} = ne(\mathbf{U}_I - \mathbf{U}_e)$ in the first term on the right-hand side of equation (1), the $\mathbf{U}_I \times \mathbf{B}$ term on the left side is cancelled to give a completely equivalent expression for the Generalized Ohm's Law as

$$\mathbf{E} + \mathbf{U}_e \times \mathbf{B} = -c\nabla \cdot \mathbf{P}_e/en + (m_e c^2/ne^2)\delta\mathbf{j}/\delta t + \eta\mathbf{j}, \quad (2)$$

where $\mathbf{U}_e$ is the velocity of an element of electron fluid.

0148-0227/05/2005JA011258$09.00

[3] Historically, magnetic field reconnection has been studied by assuming that the last term on the right-hand side of these equations dominates the other terms on the right side due to Coulomb or anomalous resistivity [*Parker*, 1957]. More recent simulations [*Birn et al.*, 2001] have considered the importance of the $\mathbf{j} \times \mathbf{B}$ term on the right-hand side of equation (1) to develop what is called "Hall MHD physics." These simulations have been validated by measurements in both space [*Deng and Matsumoto*, 2001; *Mozer et al.*, 2002; *Wygant et al.*, 2005] and the laboratory (Y. Ren et al., private communication, 2005), such that the physics on the ion skin depth scale, c/ω_{pI} ($\sim$100 km at the subsolar magnetopause), is better understood. One result of this understanding is that the tangential current required to change the direction of the reconnection magnetic field is parallel to the tangential electric field that is required for an $\mathbf{E} \times \mathbf{B}/B^2$ drift of plasma and field lines into the reconnection region such that there is a significant $\mathbf{j} \cdot \mathbf{E}$ over the ion skin depth region to convert magnetic field energy to ion energy over a large scale. However, on this scale, magnetic field lines still move with the $\mathbf{E} \times \mathbf{B}/B^2$ velocity, so the physics in the electron diffusion region on the electron skin depth scale, c/ω_{pe} ($\sim$5 km at the subsolar magnetopause), must be considered in order to understand magnetic field reconnection. The purposes of this paper are (1) to discuss the necessary conditions for the existence of electron

diffusion regions by considering magnetic field line motion from first principles, (2) to present measurements of plasma density, electric fields, and magnetic fields from the Polar satellite that show many electron diffusion regions in a filamentary magnetopause, and (3) to discuss statistical properties of these regions.

[4] This data suggests a very different geometry for the electron diffusion region in a minority of the crossings than that which is currently popular. The first results on observations of the electron diffusion region by Polar [*Mozer et al.*, 2003a] and Cluster [*Mozer et al.*, 2005] are presented elsewhere.

2. Magnetic Field Line Motion From First Principles

[5] The concept and limitations of magnetic field line motion are reviewed because these results are required to define properties of electron diffusion regions. Rigorously, magnetic field lines neither exist nor move because no experiment can be described to measure these quantities. Instead, both magnetic field lines and their motions are empirical constructs whose usefulness is that they enable one to visualize properties of the solutions to Maxwell's equations without having to solve these equations.

[6] The sole purpose of considering magnetic field line motion is to provide a means for visualizing the time evolution of the magnetic field. Among the infinite number of possible field line motions that produce the correct temporal evolution of the magnetic field [*Vasyliunas*, 1972], we will select the $\mathbf{E} \times \mathbf{B}/B^2$ velocity and consider under what conditions it produces the same temporal evolution as Maxwell's equations. To do so, we will consider separately the magnitude and the direction of a magnetic field line after it has moved with the $\mathbf{E} \times \mathbf{B}/B^2$ velocity for the time δt [*Longmire*, 1963].

2.1. Magnitude of a Magnetic Field That Evolves With Velocity $\mathbf{v} = \mathbf{E} \times \mathbf{B}/B^2$

[7] The concept of field line motion implies that a region containing a changing magnetic field experiences this change because field lines move into or out of this region and not because field lines are suddenly created or destroyed. Because field lines are conserved in this picture, they satisfy a continuity equation which, for $\mathbf{B}$ in the z-direction, is

$$\delta B_Z/\delta t + \nabla \cdot (B\mathbf{v}) = 0. \tag{3}$$

Given the field line velocity $\mathbf{v} = \mathbf{E} \times \mathbf{B}/B^2$, the components of $B\mathbf{v}$ are $(B\mathbf{v})_X = E_Y$ and $(B\mathbf{v})_Y = -E_X$, so

$$\nabla \cdot (B\mathbf{v}) = \delta E_Y/\delta x - \delta E_x/\delta y, \tag{4}$$

which is the z-component of $\nabla \times \mathbf{E}$. Because equation (3) is Faraday's law, the magnitude of the magnetic field evolves as is required by Maxwell's equations if magnetic field lines move with the $\mathbf{E} \times \mathbf{B}/B^2$ velocity. This statement is exact without approximation and in the presence or absence of plasma.

[8] It is noted that any velocity, $\mathbf{v}'$, satisfying $\nabla \cdot (B\mathbf{v}') = 0$ may be added to $\mathbf{E} \times \mathbf{B}/B^2$ without modifying equation (3). Thus there are an infinite number of magnetic field line velocities that preserve the magnitude of the magnetic field.

2.2. Direction of a Field Line That Moves With Velocity $\mathbf{v} = \mathbf{E} \times \mathbf{B}/B^2$

[9] Consider the two surfaces, S_1 and S_2 in Figure 1 that are perpendicular to the magnetic field at times t and $t + \delta t$. At time, t, a magnetic field line intersects the two surfaces at points $\mathbf{a}$ and $\mathbf{b}$. Thus the vector $(\mathbf{b} - \mathbf{a})$ is parallel to $\mathbf{B}(t)$. At the later time, $t + \delta t$, point $\mathbf{a}$ has moved along S_1 at velocity $\mathbf{E} \times \mathbf{B}/B^2(a)$ to point $\mathbf{a}'$ and it is on the illustrated magnetic field line. Meanwhile, point $\mathbf{b}$ has moved along S_2 to $\mathbf{b}'$ at velocity $\mathbf{E} \times \mathbf{B}/B^2(b)$ and it may or may not be on the field line that passes through $\mathbf{a}'$. The question is, what are the constraints on these motions that result in $\mathbf{a}'$ and $\mathbf{b}'$ being on the same magnetic field line, i.e., that result in $(\mathbf{b}' - \mathbf{a}')$ being parallel to $\mathbf{B}(t + \delta t)$?

[10] The vector $(\mathbf{b}' - \mathbf{a}') = (\mathbf{b} - \mathbf{a}) + (\mathbf{b}' - \mathbf{b}) - (\mathbf{a}' - \mathbf{a})$. The terms on the right side of this equation are $(\mathbf{b} - \mathbf{a}) = \varepsilon\mathbf{B}$ because $(\mathbf{b} - \mathbf{a})$ is parallel to $\mathbf{B}$.

$$(\mathbf{a}' - \mathbf{a}) = [\mathbf{E} \times \mathbf{B}/B^2(a)]\delta t$$

$$\begin{aligned}(\mathbf{b}' - \mathbf{b}) &= \left[\mathbf{E} \times \mathbf{B}/B^2(b)\right]\delta t \\ &= \left[\mathbf{E} \times \mathbf{B}/B^2(a) + (\mathbf{b} - \mathbf{a})\left(\delta\mathbf{E} \times \mathbf{B}/B^2(a)/\delta r\right)\right]\delta t \\ &= \left[\mathbf{E} \times \mathbf{B}/B^2(a) + \varepsilon\mathbf{B} \cdot \nabla\left(\mathbf{E} \times \mathbf{B}/B^2(a)\right)\right]\delta t,\end{aligned}$$

where r is a distance along the magnetic field line at time t.

[11] Combining terms gives

$$(\mathbf{b}' - \mathbf{a}')/\varepsilon = \mathbf{B} + \mathbf{B} \cdot \nabla(\mathbf{E} \times \mathbf{B}/B^2)\delta t. \tag{5}$$

Also

$$\mathbf{B}' = \mathbf{B}(a, t + \delta t) = \mathbf{B} + (\delta\mathbf{B}/\delta t))\delta t + ((\mathbf{E} \times \mathbf{B}/B^2) \cdot \nabla)\mathbf{B}\delta t. \tag{6}$$

The problem reduces to finding the constraints on the field line motion that are imposed by the requirement that the right side of equation (5) is parallel to the right side of equation (6) or that their cross-product is zero. To first order in δt, this gives

$$\mathbf{B} \times \left\{\delta\mathbf{B}/\delta t + \left(\mathbf{E} \times \mathbf{B}/B^2\right) \cdot \nabla)\mathbf{B} - \mathbf{B} \cdot \nabla\left(\mathbf{E} \times \mathbf{B}/B^2\right)\right\} = 0. \tag{7}$$

Using the vector identity for $\nabla \times \mathbf{M} \times \mathbf{N}$ for any two vectors $\mathbf{M}$ and $\mathbf{N}$ allows rewriting equation (7) as

$$\begin{aligned}\mathbf{B} \times \{&\delta\mathbf{B}/\delta t + \nabla \times \left(\mathbf{B} \times \left(\mathbf{E} \times \mathbf{B}/B^2\right)\right) + \mathbf{B}\left(\nabla \cdot \left(\mathbf{E} \times \mathbf{B}/B^2\right)\right) \\ &- (\mathbf{E} \times \mathbf{B}/B^2)\nabla \cdot \mathbf{B}\} = 0.\end{aligned} \tag{8}$$

The last term on the right is zero because $\nabla \cdot \mathbf{B} = 0$ and the next to last term may be omitted because it is parallel to $\mathbf{B}$. Because $\mathbf{B} \times (\mathbf{E} \times \mathbf{B}/B^2) = \mathbf{E} - \mathbf{E}_{\|}$ and $\delta\mathbf{B}/\delta t = -\nabla \times \mathbf{E}$, equation (8) becomes

$$\mathbf{B} \times (\nabla \times \mathbf{E}_{\|}) = 0 \tag{9}$$

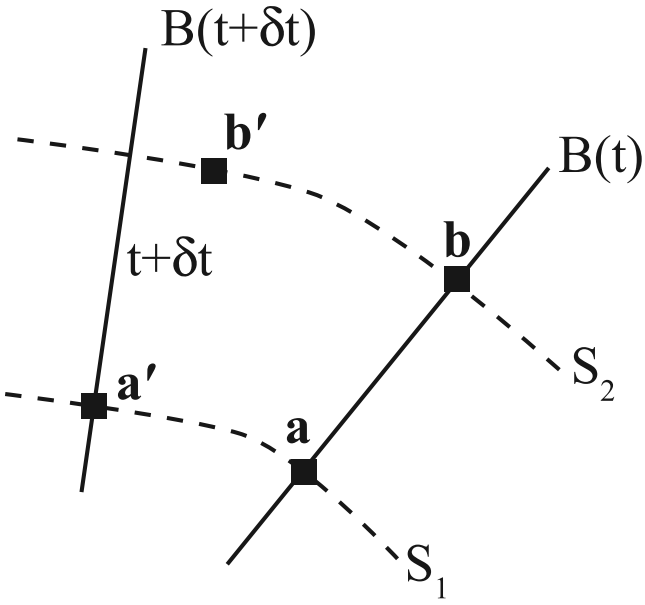

Figure 1. Geometry of moving magnetic field lines.

This is the condition that preserves the direction of the magnetic field during its $\mathbf{E} \times \mathbf{B}/B^2$ motion. It may be satisfied in four ways. The first is for

$$\mathbf{E}_{\|} = 0. \tag{10}$$

The second is for

$$\mathbf{B} = 0. \tag{11}$$

The third is for

$$\nabla \times \mathbf{E}_{\|} = 0. \tag{12}$$

The fourth is obtained by setting $\mathbf{E}_{\|} = \mathbf{B}(E_{\|}/B)$ and expanding equation (9) to obtain [*Scudder*, 1997]

$$\mathbf{B} \cdot (\nabla \times \mathbf{B}) = 0. \tag{13}$$

Thus when $E_{\|} \neq 0$, magnetic field lines moving with $\mathbf{E} \times \mathbf{B}/B^2$ do not produce the same time evolution of the magnetic field direction as do Maxwell's equations unless $B = 0$, or $\nabla \times \mathbf{E}_{\|} = 0$, or $\mathbf{B} \cdot (\nabla \times \mathbf{B}) = 0$. Because none of these conditions are likely and, in any case, the first condition has not been met by any of the events in this paper and the other two conditions cannot be tested with data from a single spacecraft (or many spacecraft) because they involve spatial derivatives, we will assume that the condition for valid field line motion is the absence of $E_{\|}$. In a probably small percentage of cases, this assumption may be invalid. However, it is consistent with the present data set because cases with $E_{\|} \neq 0$ also contain topological changes of $\mathbf{E} \times \mathbf{B}/B^2$, which would be unlikely if the field lines moved at $\mathbf{E} \times \mathbf{B}/B^2$.

[12] The existence and/or properties of plasma did not enter into the equation (9) requirement that field line motion at $\mathbf{E} \times \mathbf{B}/B^2$ produces the same result as do Maxwell's equations. Thus for example, one may consider that magnetic field lines move with $\mathbf{E} \times \mathbf{B}/B^2$ in a vacuum when equation (9) is satisfied. Or, one may consider that field lines move with $\mathbf{E} \times \mathbf{B}/B^2$ in a plasma having no parallel electric field but, in which, the electron and ion fluids do not move with this velocity because there is a perpendicular pressure gradient.

3. Necessary Conditions for Observing the Electron Diffusion Region

[13] The electron diffusion region is a region in which the temporal evolution of the magnetic field by field lines moving with the $\mathbf{E} \times \mathbf{B}/B^2$ velocity does not agree with that obtained from Maxwell's equations. In such a region, terrestrial and interplanetary magnetic field lines may connect to change the magnetic field topology outside of this region, where the field lines do move with the $\mathbf{E} \times \mathbf{B}/B^2$ velocity. The properties of the electron diffusion region that may be sought in experimental data are as follows.

[14] 1. The parallel electric field must be nonzero. Oppositely oriented magnetic field lines that move toward each other with the $\mathbf{E} \times \mathbf{B}/B^2$ velocity will move right through each other if they continued at this velocity. Because this situation neither results in reconnection nor is consistent with Maxwell's equations, such field lines must not move with the $\mathbf{E} \times \mathbf{B}/B^2$ velocity in the electron diffusion region. Thus a necessary condition for the existence of the electron diffusion region is that the parallel electric field is nonzero (see discussion following equation (13)). Because the left side of equation (2) is nonzero in this case, one or more of the terms on the right side of this equation must also be nonzero. Previous measurements suggest that the pressure gradient term may dominate [*Mozer et al.*, 2003a; *Mozer et al.*, 2005].

[15] 2. The thickness of the region must be the order of the electron skin depth, c/ω_{pe}. *Vasyliunas* [1975] has shown that the electron diffusion region has a thickness that is $\sim c/\omega_{pe}$, which is the order of 4 km at the subsolar magnetopause.

[16] 3. The perpendicular electric field must be large. The reconnection electric field associated with a reconnection rate $\sim 0.1 v_{Alfven}$ is ~ 0.5 mV/m. The perpendicular electric field must be large compared to this value for the electron diffusion region to exert an important influence on reconnection.

[17] 4. The $\mathbf{j} \cdot \mathbf{E}$ must be large. The electron diffusion region is a site of conversion of magnetic field energy, so $\mathbf{j} \cdot \mathbf{E}$ must be large.

[18] 5. Accelerated electrons must be produced in the electron diffusion region. The electromagnetic energy conversion should produce accelerated electron beams.

[19] 6. The electron diffusion region must be a topological boundary that separates regions having different $\mathbf{E} \times \mathbf{B}/B^2$ flows. In two-dimensional reconnection, plasma and magnetic field lines $\mathbf{E} \times \mathbf{B}/B^2$ flow in from the left and right and out the top and bottom of the geometry. While the $\mathbf{E} \times \mathbf{B}/B^2$ flow in realistic geometries is expected to be more complex, it should still be the case that the electron diffusion region is a boundary separating different flow topologies.

[20] Simulations [*Shay et al.*, 2001] and measurements [*Mozer et al.*, 2002; *Mozer et al.*, 2005] show that these

same properties occur in the separatrix region of reconnection events. For this reason and because other regions having these same properties will be shown to exist throughout the reconnection current layer, the operational definition of "electron diffusion region" in this paper is any region that satisfies the above six criteria. Any such electron diffusion region contains one or more nonzero terms on the right hand side of equation (2). In a collisionless plasma, this requires that the inertia term or the divergence of the pressure tensor or both be nonzero. In this sense, all electron diffusion regions reported in this paper contain the same basic microphysics, although the details associated with the electron physics can differ in different examples or different geometries. Because there is no prohibition against reconnection occurring in finite magnetic fields, there are no limitations on the field strength or the electron beta that are imposed in the following search for electron diffusion regions.

[21] The data from the Polar satellite allow determination of the parallel electric field because Polar contains a three-component E-field measurement. This contrasts with the two-component data from the Cluster satellite that do not permit determination of the parallel electric field. However, the EDI experiment on Cluster [*Paschmann et al.*, 1997] produces measurements of natural electrons at two pitch angles with an 8 ms time resolution, thereby providing accelerated electron data that satisfies criterion 5, above [*Mozer et al.*, 2005]. Thus the combination of data from the two spacecraft satisfies all of the above criteria.

4. Measurements of the Parallel Electric Field on Polar

[22] From February through mid-May in 2001, 2002, and 2003, the 9.5 R_E geocentric apogee of the Polar satellite was at low latitudes on the dayside of the magnetosphere. Electric fields at magnetopause crossings were examined during these times for candidate electron diffusion region events. Because a nonzero parallel electric field is required, the parallel electric field measurement was closely scrutinized. It may be uncertain because (1) it is as small as 10% of the perpendicular electric field, so geometric misalignments can produce apparent parallel electric fields, (2) the magnetic field is not measured with the time resolution of the electric field, so the B-field is linearly interpolated to the times of E-field measurements. If the rapidly changing magnetic field does not vary linearly, apparent parallel electric fields can result, (3) the short, spin-axis electric field measurement [*Harvey et al.*, 1995] is uncertain due to its proximity to perturbations from the spacecraft. This may introduce noise in the parallel field estimate that can be comparable to the observed parallel field, depending on the geometry of the situation. This is the source of the largest uncertainty in the parallel electric field measurement.

[23] Because the Polar spacecraft was in a cartwheel mode, one of the pair of on-axis sensors was shadowed by the spacecraft in the vicinity of the dawn-dusk orbit, and the resulting on-axis data is not usable. However, in the noon-midnight orbit, there is a high level of symmetry between these sensors, the spacecraft, its photoemission, and the Sun. This causes any perturbation from photoemission, for example, to be the "same" on the two on-axis sensors, so this perturbation cancels when the potential difference is measured. However, one of the on-axis sensors is closer than the other to the center of the 1/r potential from the charged spacecraft because the despun platform extends on one side of the spacecraft to spoil the axial symmetry. For this reason, it is necessary to subtract ~200 mV from the measured potential difference along the spin axis to obtain a field that is small in regions where the spin-plane-measured fields are small. Other than adjusting this offset, there are no special corrections made to the on-axis measurements.

[24] Figure 2 illustrates the technique for validating the parallel electric field measurement. The data are presented in a field-aligned coordinate system in which the Z-axis is parallel to the magnetic field direction while the X-axis is perpendicular to **B** in the plane containing the magnetic field line and it is positive inward. The Y-axis defines the third component of this right hand coordinate system by being perpendicular to **B** and pointing generally in the westward direction. The field components in this coordinate system are obtained in three ways: (1) by using the measured three components of the electric field, (2) by discarding the on-axis measurement and assuming the parallel electric field is zero, and (3) by discarding the on-axis measurement and assuming that the component of the electric field in this direction is zero.

[25] Figures 2a, 2b, and 2c give the X-component of the electric field computed in the three ways, Figures 2d, 2e, and 2f give the Y-component, and Figures 2g and 2h give the Z-component (the Z-component computed under the assumption that $\mathbf{E}\cdot\mathbf{B} = 0$ is not given because it is zero). The figure contains 4 s of data at a geocentric distance of 9.47 Earth radii, magnetic local time of 1320, and magnetic latitude of −14.2 degrees. Note that the scales of the electric field plots differ for the different field components. The values of E_X computed by the three methods are essentially identical because the X-direction in magnetic field aligned coordinates happened to be perpendicular to the spacecraft spin axis. The value of E_Y computed by assuming that the on-axis field was zero (Figure 2f) is small because the Y-direction was nearly parallel to the spin axis. The parallel electric fields in Figures 2g and 2h are nonzero and similar because the parallel electric field comes mainly from measurements made by the long spin plane sensors. E_Y obtained from direct measurements (Figure 2d) and from assuming that the parallel electric field was zero (Figure 2e) differ by factors as large as four. This is strong evidence that the measured parallel electric field is real because the Y-component requires a major adjustment if it is to be compatible with the assumption that the parallel electric field was zero.

[26] Examples satisfying the above criteria for yielding an acceptable parallel field were found in more than 100 of the ~1000 cases that were examined.

5. Further Examples of Electron Diffusion Regions

[27] Figure 3 gives the plasma density, the magnetic field, and the components of $\mathbf{E} \times \mathbf{B}/B^2$ for the same 4 s interval as in Figure 2. The plasma density in Figure 3a decreased from about 1.5 to 0.1 cm^{-3} during the fraction of a second that

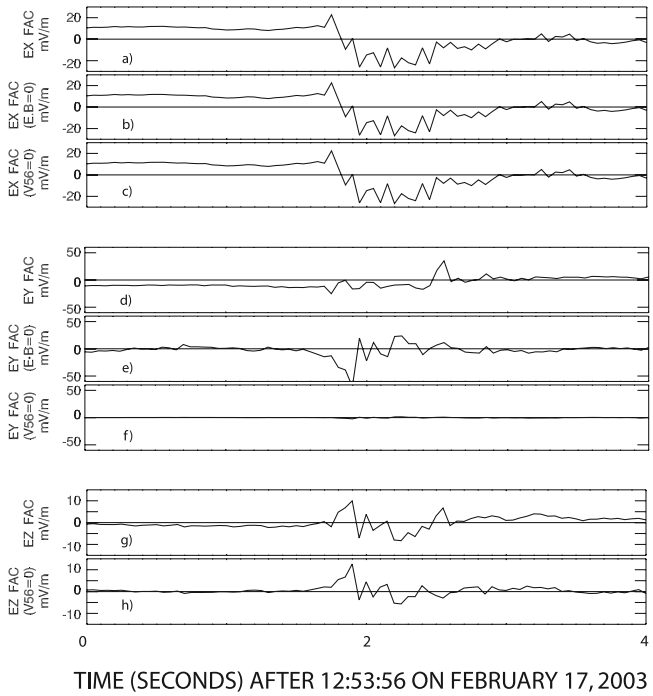

Figure 2. Electric field components in a magnetic-field-aligned coordinate system that illustrate the method of validating the parallel electric field measurement.

the electron diffusion region was crossed. The magnetic field components of Figures 3b, 3c, and 3d (plotted with different zero level suppressions) show that the spacecraft was at or near the magnetospheric separatrix because the Z-component had the magnetospheric sign and magnitude. The components of $\mathbf{E} \times \mathbf{B}/B^2$, illustrated in Figures 3f, 3g, and 3h changed across the diffusion region by as much as 150 km/s, indicating that the fields and flows on one side of the boundary were independent of those on the other side. (The components of $\mathbf{E} \times \mathbf{B}/B^2$ have been deleted in the region of the parallel electric field because they are not meaningful in terms of either electron or field line flow.) The electron beta for this event was about 0.005. The average parallel electric field of Figure 2 was about 30% of the perpendicular field but there were times when the parallel field exceeded the perpendicular field. The temporal variations of the field components were at the 25 ms resolution of the measurement. Boundary speeds have been measured to vary between ~10 and 100 km/s [*Berchem and Russell*, 1982]. Over this range of speeds, the thickness of a 25 ms spiky field event would be less than several kilometers, which is less than the 5–15 km electron skin depth.

[28] The total magnetic field of Figure 3e did not change across the electron diffusion region. Thus the steps in B_Y and B_Z in Figures 3c and 3d must have been due to field-aligned currents. For a magnetic field change of 9 nT in 0.7 s and an assumed boundary speed of 50 km/s, Ampere's law gives a parallel current density of 0.1 μamp/m^2. Combining this current density with an average parallel electric field of 8 mV/m and plasma density of 0.2 cm^{-3} gives $j_{ll}E_{ll}/n \approx 50$ keV/particle s. Thus a typical electron that receives this energy while residing in the electron diffusion region for ~5 ms will gain a few hundred eV of energy.

[29] An extremely rare example of an electron diffusion region at the magnetosheath separatrix is given in Figures 4 and 5 at a time when the spacecraft was at an altitude of 9.38 R_E, magnetic local time of 1145, and magnetic latitude of 6.25 degrees. Prior to the event of interest in Figure 5, the Z-component of the magnetic field in Figure 4d changed from +80 nT to −80 nT in steps, signifying the crossing of a magnetopause containing a filamentary current. It is noted that the magnetic field in GSE coordinates in this figure is nearly in the minimum variance coordinates because B_X of Figure 4b is small and nearly nonchanging, while the maximum variance occurs in B_Z. Also, this was a rotational discontinuity with a mostly parallel current because the total field of Figure 4e did not change very much. The data of Figure 5 were collected at the time of the dashed line in Figure 4, during which the magnetic field was near its magnetosheath value. Figure 5a shows that the magnetosheath plasma density was unusually low and that it changed significantly as the electron diffusion region was crossed. Figures 5b, 5c, and 5d give the electric field components in the field-aligned coordinate system. No change of $\mathbf{E} \times \mathbf{B}/B^2$ greater than about 50 km/s was observed at this crossing. The spiky electric field structures

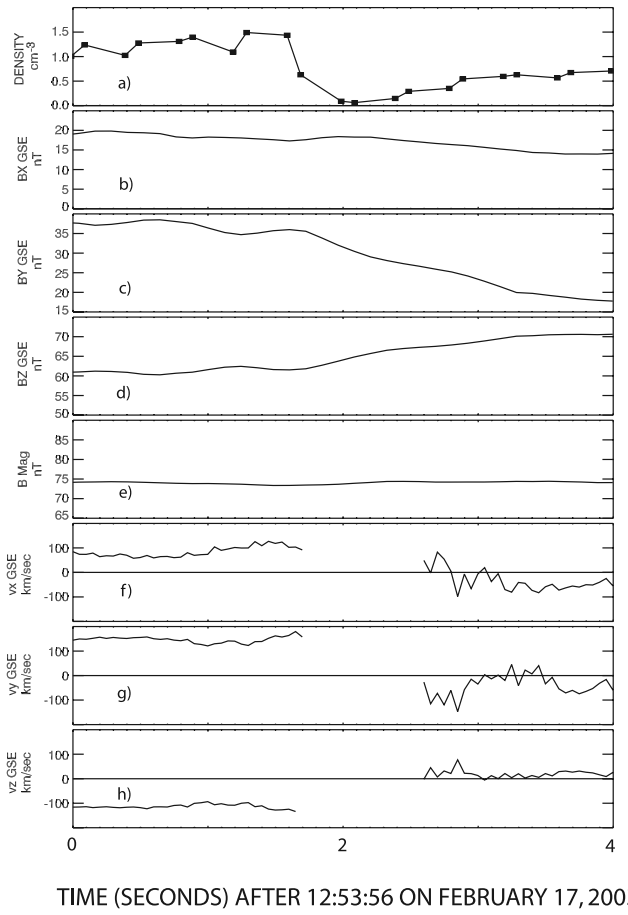

Figure 3. Plasma density, magnetic field, and components of $\mathbf{E} \times \mathbf{B}/B^2$ during the time interval illustrated in Figure 2.

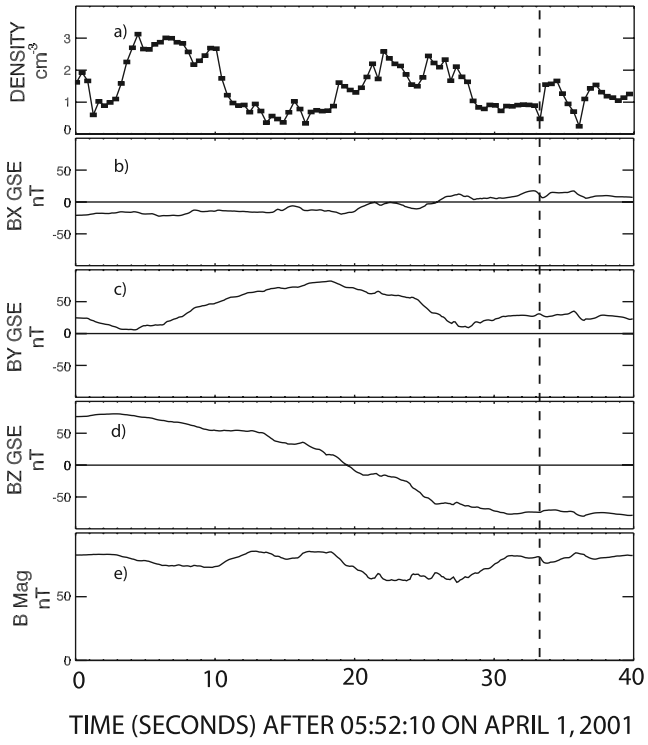

Figure 4. Magnetic field and plasma density during a magnetopause crossing from the magnetosphere to the magnetosheath.

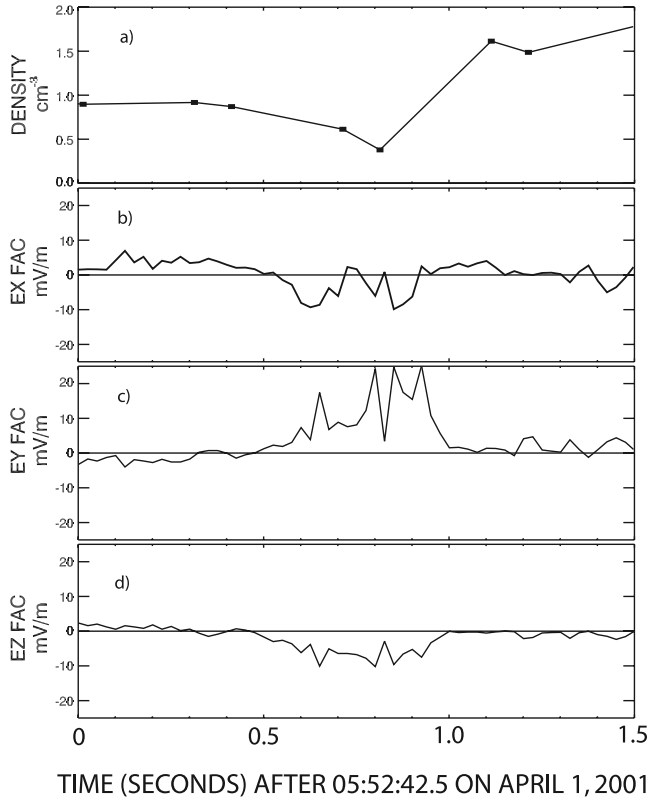

Figure 5. Field measurements made as a magnetosheath electron diffusion region passed over the Polar spacecraft.

had thicknesses less than or the order of the electron skin depth. The electron plasma beta was about 0.01 during this event. For an assumed boundary speed of 50 km/s, $j_{ll}E_{ll}/n$ was about 25 keV/particle s with an uncertainty of at least a factor of two because the boundary speed is not known and the magnetic field and plasma density were not measured with sufficient time resolution.

[30] An example of an electron diffusion region near the center of the magnetopause is described in Figures 6 and 7. The spacecraft was at an altitude of 8.92 R_E, magnetic local time of 1325, and magnetic latitude of 37.67 degrees. Figure 6 gives the plasma density (Figure 6a), the three components of the magnetic field (Figures 6b, 6c, and 6d), and the total magnetic field intensity (Figure 6e). During the 22 s interval of this figure, the density increased from a magnetospheric value of $\sim$1 cm^{-3} to the magnetosheath value of $\sim$18 cm^{-3}, while the Z-component of the magnetic field decreased from its $\sim$55 nT magnetospheric value to the $-$30 nT magnetosheath value. Near the center of the crossing, at the 8 nT minimum of the total magnetic field, the plasma density decreased and then increased by factors of about 4 in less than 1 s. This region is expanded in the 6 s plot of Figure 7, which also includes the components of the electric field in field-aligned coordinates and $\mathbf{E} \times \mathbf{B}/B^2$ in GSE coordinates. (The components of $\mathbf{E} \times \mathbf{B}/B^2$ have been deleted in the region of the parallel electric field because they are not meaningful.) Although the magnitude of the perpendicular electric field was small compared to typical values (Figure 7b and 7c), the parallel field was the typical 5–8 mV/m (Figure 7d) and it was larger than the perpendicular field at the two large plasma density changes. The $\mathbf{E} \times \mathbf{B}/B^2$ components of Figures 7e, 7f, and 7g show that the electron and magnetic field perpendicular flows changed by $\sim$100 km/s across the

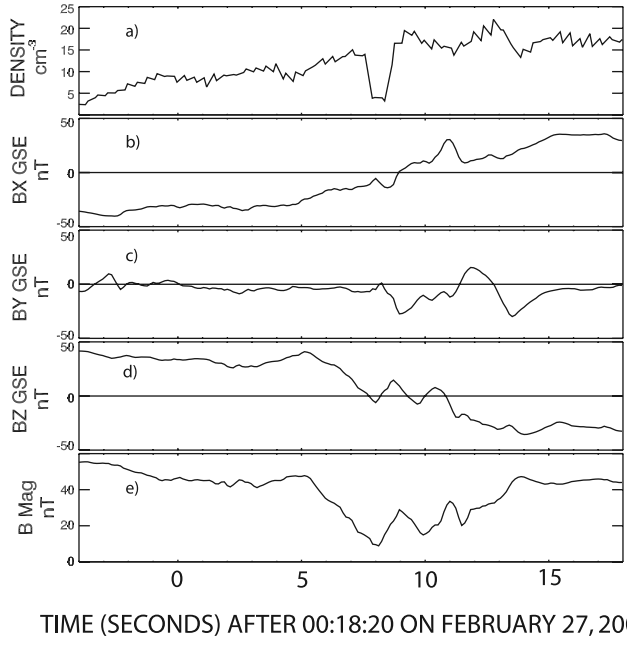

Figure 6. Magnetic field components and plasma density measured at an electron diffusion region near the center of the magnetopause.

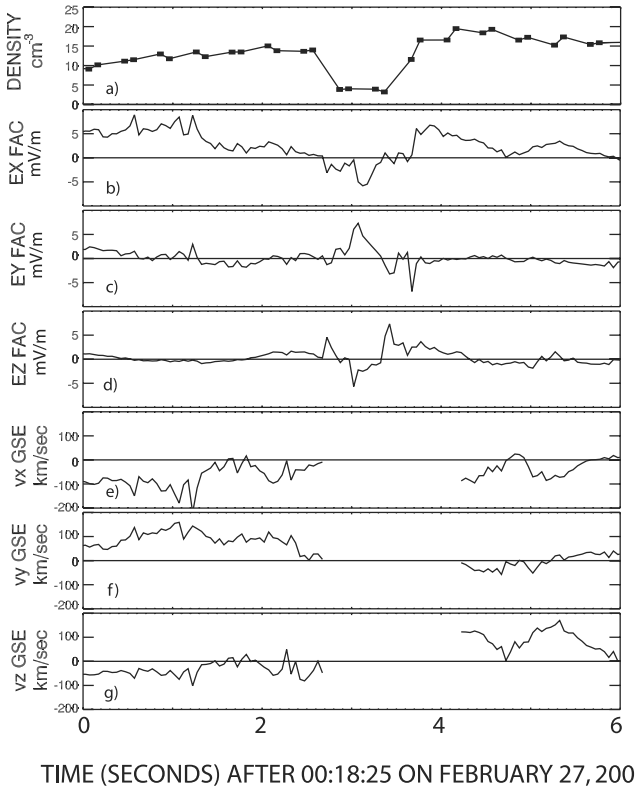

Figure 7. Electric field and $\mathbf{E} \times \mathbf{B}/B^2$ flow measurements made at an electron diffusion region located near the center of the magnetopause.

electron diffusion region, signifying that the fields on the two sides of the boundary were uncoupled. The electron beta during this event was greater than 2.

6. Statistics of Subsolar Electron Diffusion Regions

[31] During the 3 year search for subsolar electron diffusion regions, 117 events satisfying rigorous criteria on the parallel electric field were identified. These events do not occur randomly in time; rather they come in bunches. For example, 70 of the 117 events were found in 12 of the ~400 orbits that were examined. Most of the events occurred in current filaments and were associated with significant changes of the plasma density. Most of the magnetopause crossings did not yield verifiable electron diffusion regions.

[32] Figure 8 gives the electron diffusion region locations in magnetic latitude and magnetic local time. The subsolar point is in the center of this plot and events were found at all local times and latitudes at which the spacecraft encountered the magnetopause. This includes the region from 0800 to 1600 in magnetic local time and −40 to +40 degrees of magnetic latitude.

[33] Figure 9 shows the angle between the asymptotic magnetosheath and magnetospheric magnetic field vectors as a function of magnetic latitude for the magnetopause reconnection events that contained electron diffusion regions. A wide range of angles was observed at all latitudes reached by the spacecraft trajectory. The apparent number of large angles may be a selection effect because the signature of such crossings is much clearer than for those having a small angle. Some of the small angles may be inaccurate because the turbulence in the magnetic field made such measurements uncertain.

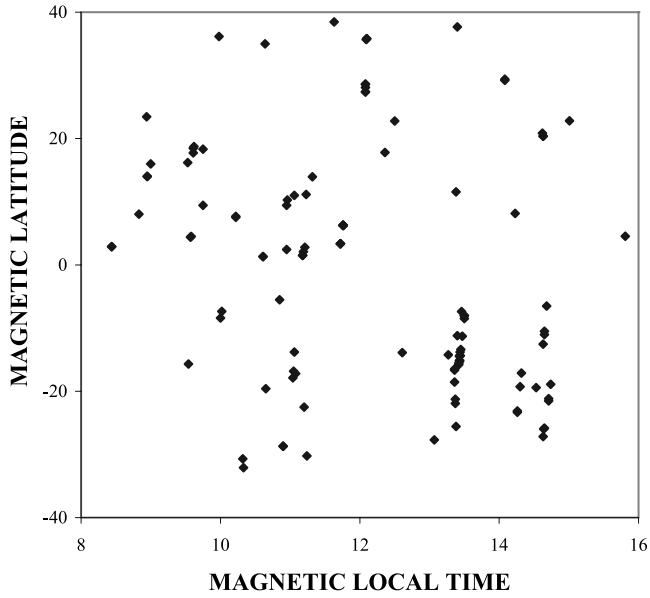

Figure 8. Locations in magnetic local time and magnetic latitude of electron diffusion region events.

[34] A histogram of the perpendicular electric field magnitudes in electron diffusion regions is given in Figure 10. While the observed fields ranged up to 100 mV/m, the average perpendicular electric field was 38 mV/m, which is one or two orders of magnitude larger than the reconnection electric field found in theories and simulations.

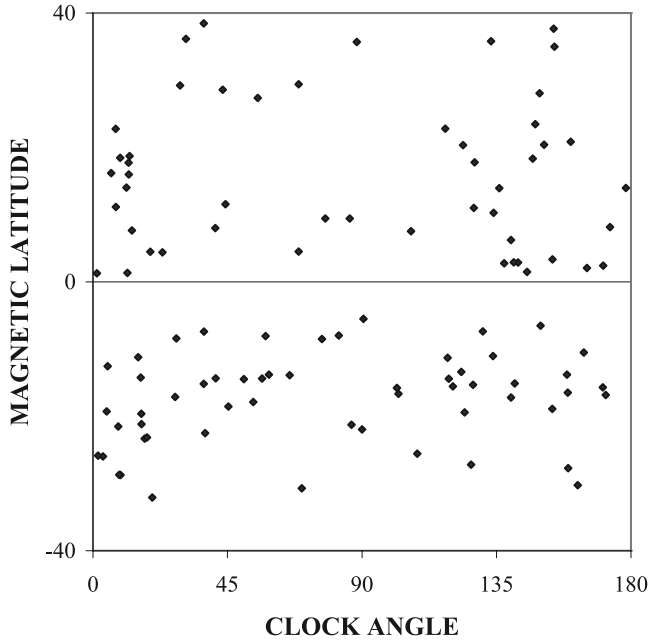

Figure 9. The angle between the asymptotic magnetosheath and magnetospheric magnetic field vectors versus the magnetic latitude of the reconnecting magnetopauses in which electron diffusion regions were found.

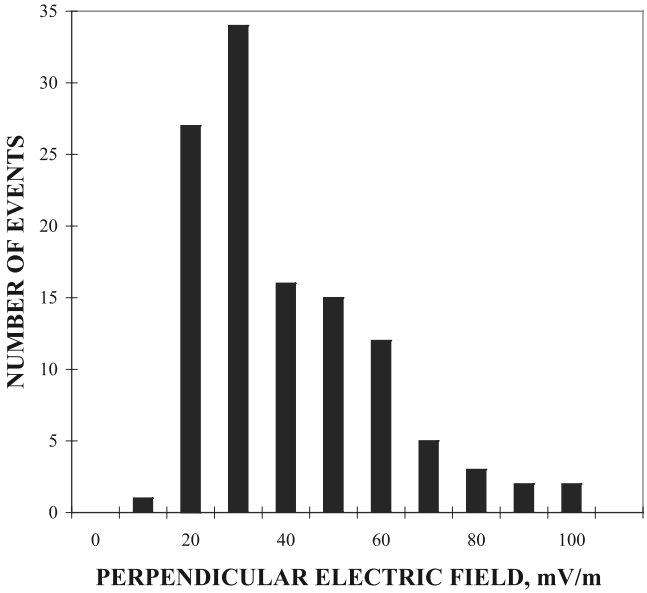

Figure 10. Perpendicular electric field magnitudes measured in electron diffusion regions.

[35] The ratio of the parallel to perpendicular electric fields is plotted in Figure 11. The smallest parallel electric fields were 10% of the perpendicular field because the criteria on an event included the requirement that the parallel field be at least this large in order that geometric errors could not produce an apparent parallel field. This figure gives the average of the ratio over each event. However, it is emphasized that the magnitude of the instantaneous parallel electric field exceeded that of the perpendicular field at some point in the event for a significant fraction of the events.

[36] Values of the Z-component of the magnetic field in GSE coordinates are given in the histogram of Figure 12.

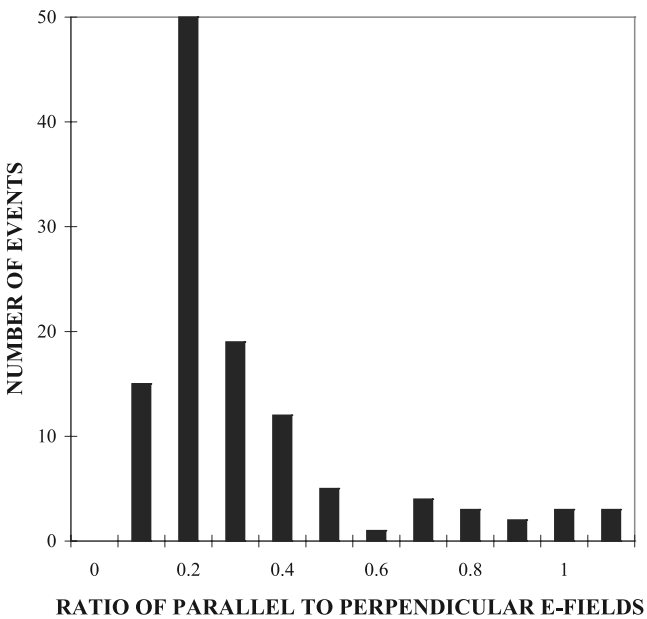

Figure 11. The ratio of the parallel electric field to the perpendicular electric field in electron diffusion regions.

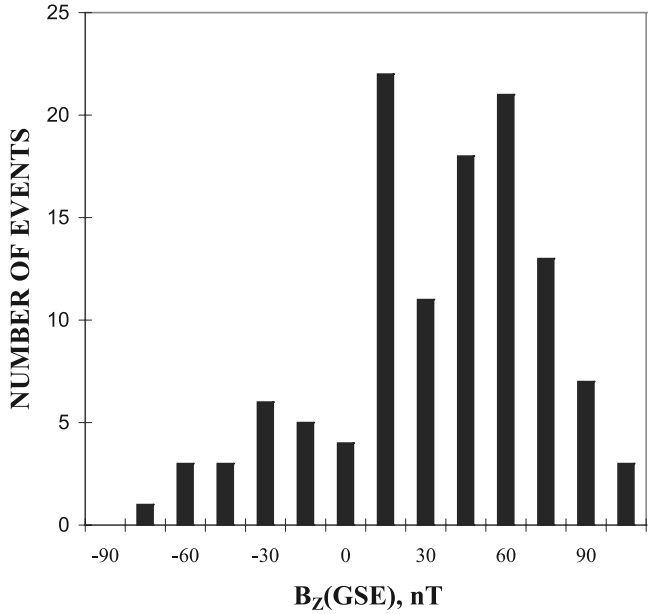

Figure 12. Reconnection magnetic field components measured in electron diffusion regions.

This component serves as a proxy for the reconnection magnetic field. It was positive more than 81% of the time, indicating that most of the electron diffusion regions were found on the magnetospheric side of the magnetopause. This is because more than half of the events were found at the magnetospheric separatrix.

[37] The total magnetic field strength in the many events is plotted in the histogram of Figure 13. None of the events occurred in magnetic fields smaller than about 10 nT and more than half of the events occurred in fields greater than 70 nT.

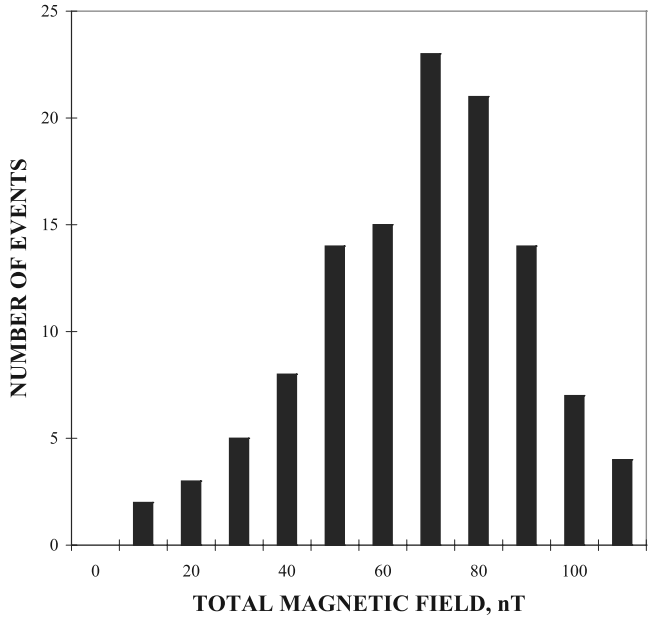

Figure 13. The total magnetic field measured in electron diffusion regions.

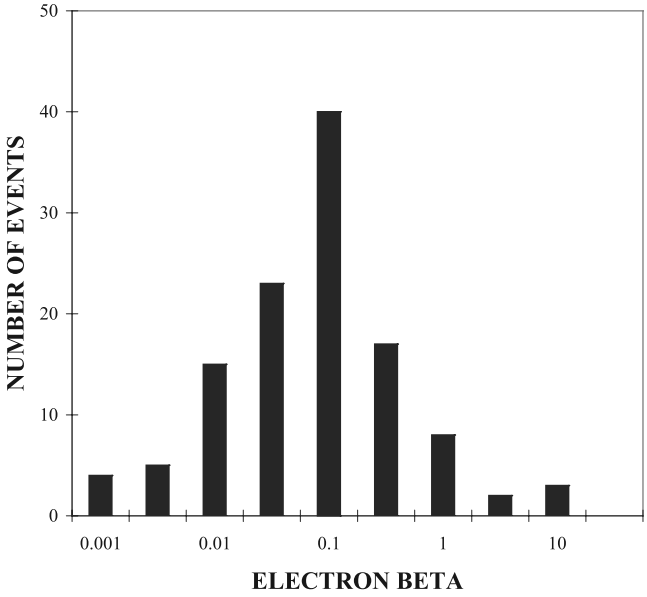

Figure 14. The plasma electron beta measured in electron diffusion regions.

[38] The distribution of plasma electron betas is plotted in Figure 14. These values were determined by assuming that the electron characteristic energy was 200 eV. Even with an uncertainty in this temperature estimate as great as a factor of four, fewer than 15% of the events had an electron beta greater than unity.

[39] Figure 15 presents a histogram of the ratio of the electron gyroradius to the electron skin depth for an assumed electron energy of 200 eV. The average ratio is about 0.2. Because the average thickness of the electric field spikes in the electron diffusion region in several examples is 30% of the electron skin depth [*Mozer et al.*, 2005], the gyroradius can be comparable to the thickness of large electric field regions and this might exert a significant impact on the microphysics.

7. Discussion

[40] By definition, the necessary conditions for the observation of an electron diffusion region are that the parallel electric field is nonzero, $\mathbf{j}\cdot\mathbf{E}$ is large, the thickness of the region is $\sim c/\omega_{pe}$, the perpendicular electric field is large compared to the typical reconnection electric field, and the region is a boundary separating different electron and magnetic field line flows on its two sides. Polar satellite events are shown to satisfy all these criteria. An additional criterion is that accelerated electrons should be observed in the electron diffusion region. The Polar particle instruments do not have the time resolution to test this requirement. However, Cluster data have shown the existence of accelerated electrons and have produced an estimate of the average thickness of the electron diffusion region as $\sim 0.3c/\omega_{pe}$ in the direction of its motion and more than 1000 kilometers in the plane perpendicular to its motion [*Mozer et al.*, 2005]. Thus the combination of the Polar and Cluster data satisfy the requirements to identify the objects studied in this paper as electron diffusion regions.

[41] A possible explanation for the more frequent occurrence of electron diffusion regions at the magnetospheric side of the magnetopause is that the current imposed on the local region by its filamentary nature is too large to be carried by the low-density plasma near the magnetosphere, so parallel electric fields and the associated microphysics are required to maintain current continuity.

[42] As shown in Figures 3 through 7, the majority of the observed electron diffusion regions were accompanied by plasma density decreases. Because these variations occurred often in the 117 events, they may have been spatial rather than temporal. In this case, the density decreases signified spatial variations of the electron pressure whose magnitudes may have been sufficient to balance the nonzero nature of the left side of equation (2) by the pressure tensor term on the right side of that equation.

[43] It is again noted that the electron beta was less than one for more than 85% of the electron diffusion regions and that most events occurred in filamentary currents in which the plasma density was depleted. These features will be significant in any theory of these regions.

[44] The picture resulting from this data is of a magnetopause that is highly structured and filamentary and that contains many electron diffusion regions, which is similar to that described in several simulations [*Ma and Bhattacharjee*, 1996, 1999; *Onofri et al.*, 2004; *Karimabadi et al.*, 2005; J. F. Drake, private communication, 2005] and very different from a linear, laminar, symmetric structure sometimes considered in theories or simulations. However, it is emphasized that magnetopauses such as these were found less than 20% of the time. Of the ~400 orbits searched in three years of Polar data, 70 of 117 events occurred during 12 orbits.

[45] These events having multiple electron diffusion regions contradict the model of a single reconnection region at the center of the magnetopause, from which the magnetic

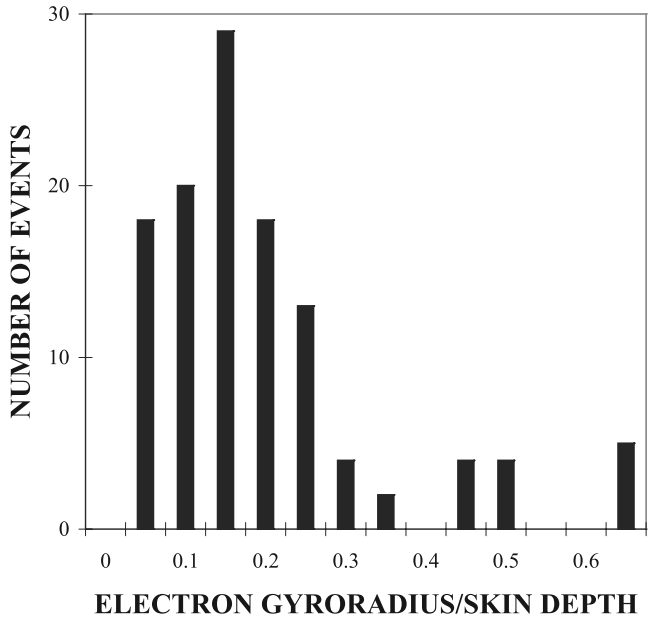

Figure 15. The ratio of the electron gyroradius to the electron skin depth for an assumed electron energy of 200 eV.

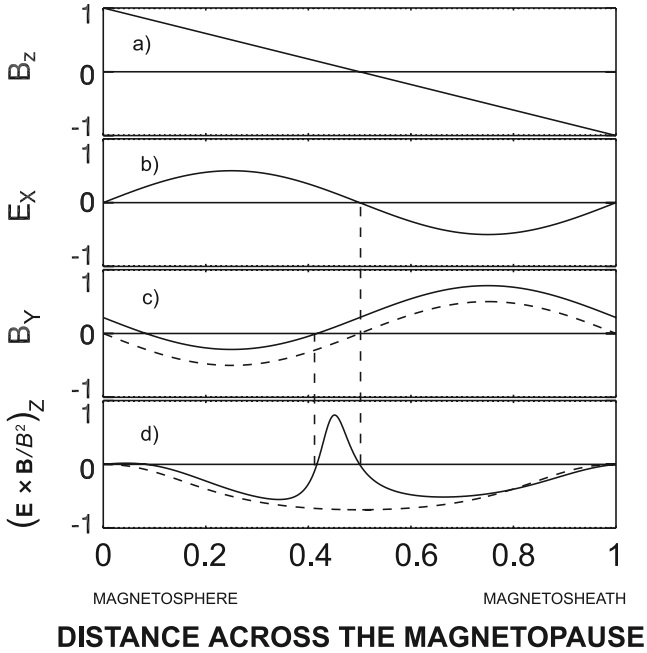

Figure 16. Electric and magnetic fields in an idealized Hall MHD model of the magnetopause, showing that postreconnection flow toward the x-line occurs when the guide magnetic field is nonzero.

field and plasma are slingshot into the outflow region. Moreover, this slingshot model is inconsistent with the measured result of Hall MHD physics that the postreconnection electron and field line flow can be toward the x-line [*Mozer et al.*, 2003b]. This result is illustrated in Figure 16, which gives field components in an idealized Hall MHD model [*Birn et al.*, 2001] in which the reconnection magnetic field, B_Z, of Figure 16a changes from positive at the magnetosphere to negative at the magnetosheath. Figure 16b and 16c give the normal E_X and the tangential B_Y, both having the bipolar structures found in Hall MHD. The magnetic field component of Figure 16c is plotted twice, once as a dashed curve having no guide magnetic field and a second time as a solid curve with a guide field that is 1/8 of the reconnection magnetic field. The z-component of $\mathbf{E} \times \mathbf{B}/B^2$ is the postreconnection flow and it is plotted in Figure 16d, except for singular points that have been removed. It is equal to $(E_X B_Y - E_Y B_X)/(B_X^2 + B_Y^2 + B_Z^2)$. Because E_Y is a few percent of E_X and B_X is a few percent of B_Y, the E_Y and B_X terms do not influence the overall behavior of the $\mathbf{E} \times \mathbf{B}/B^2$ flow and they are neglected in computing Figure 16d. With a zero guide field, E_X and B_Y have opposite signs everywhere in the reconnection layer, so their negative product gives downward outflow everywhere, as is shown by the dashed curve in Figure 16d. (The outflow is downward because the bipolar B_Y has the sign appropriate to a region below the x-line.) When the guide field is nonzero, the dashed vertical lines in Figure 16 encompass a region in which E_X and B_Y have the same sign. This results in a flow toward the x-line in the outflow region, which has been observed [*Mozer et al.*, 2002; *Mozer et al.*, 2003b] and which contradicts the slingshot model of the electron and magnetic field line flows in the postreconnection region. Thus model concepts of magnetopause structure and dynamics must be revised in view of new experimental and theoretical results. It is also noted that an event on the Cluster satellites similar to those discussed herein has been studied by *Andre et al.* [2004].

[46] **Acknowledgments.** This work was performed under NASA grant FDNAG5-11733.

[47] Lou-Chuang Lee thanks Zhi-wei Ma and Goetz Paschmann for their assistance in evaluating this paper.

References

Andre, M., A. Vaivads, S. C. Buchert, A. N. Fazakerley, and A. Lahiff (2004), Thin electron-scale layers at the magnetopause, *Geophys. Res. Lett.*, *31*, L06502, doi:10.1029/2003GL019252.

Berchem, J., and C. T. Russell (1982), The thickness of the magnetopause current layer: ISEE 1 and 2 observations, *J. Geophys. Res.*, *87*, 2108.

Birn, J., et al. (2001), Geospace environmental modeling (GEM) magnetic reconnection challenge, *J. Geophys. Res.*, *106*, 3715.

Deng, X. H., and H. Matsumoto (2001), Rapid magnetic reconnection in the Earth's magnetosphere mediated by whistler waves, *Nature*, *410*, 557.

Harvey, P., et al. (1995), The electric field instrument on the Polar satellite, *Space Sci. Rev.*, *79*, 583.

Karimabadi, H., W. Daughton, and K. B. Quest (2005), Anti-parallel versus component merging at the magnetopause: Current bifurcation and intermittent reconnection, *J. Geophys. Res.*, *110*, A03213, doi:10.1029/2004JA010750.

Longmire, C. L. (1963), *Elementary Plasma Physics*, Interscience, New York.

Ma, Z. W., and A. Bhattacharjee (1996), Fast impulsive reconnection and current sheet intensification due to electron pressure gradients in semi-collisional plasmas, *Geophys. Res. Lett.*, *23*, 1673.

Ma, Z. W., and A. Bhattacharjee (1999), Sudden disruption of a thin current sheet in collisionless Hall magnetohydrodynamics due to secondary tearing and coalescence instabilities, *Geophys. Res. Lett.*, *26*, 3337.

Mozer, F. S., S. D. Bale, and T. D. Phan (2002), Evidence of diffusion regions at a sub-solar magnetopause crossing, *Phys. Rev. Lett.*, *89*, 015002, doi:10.1103/PhysRevLett.89.015002.

Mozer, F. S., S. D. Bale, T. D. Phan, and J. A. Osborne (2003a), Observations of electron diffusion regions at the subsolar magnetopause, *Phys. Rev. Lett.*, *91*, 245002.

Mozer, F. S., T. D. Phan, and S. D. Bale (2003b), The complex structure of the reconnecting magnetopause, *Phys. Plasmas*, *10*, 2480.

Mozer, F. S., S. D. Bale, J. P. McFadden, and R. B. Torbert (2005), New features of electron diffusion regions observed at sub-solar magnetic field reconnection sites, Geophys. Res. Lett., *32*, L24102, doi:10.1029/2005GL024092.

Onofri, M., L. Primavera, F. Malara, and P. Veltri (2004), Three-dimensional simulations of magnetic reconnection in slab geometry, *Phys. Plasmas*, *11*, 4830.

Parker, E. N. (1957), Sweet's mechanism for merging magnetic fields in conducting fluids, *J. Geophys. Res.*, *62*, 509.

Paschmann, G., et al. (1997), The electron drift instrument for Cluster, *Space Sci. Rev.*, *79*, 233.

Scudder, J. D. (1997), Theoretical approaches to the description of magnetic merging: The need for finite β_e, anisotropic, ambipolar Hall MHD, *Space Sci. Rev.*, *80*, 235.

Shay, M. A., J. F. Drake, B. N. Rogers, and R. E. Denton (2001), Alfvenic collisionless magnetic reconnection and the Hall term, *J. Geophys. Res.*, *106*, 3759.

Spitzer, L., Jr. (1956), *Physics of Fully Ionized Gases, Interscience Tracts on Phys. and Astron.*, edited by R. E. Marshak, Interscience, New York.

Vasyliunas, V. M. (1972), Nonuniqueness of magnetic field line motion, *J. Geophys. Res.*, *77*, 6271.

Vasyliunas, V. M. (1975), Theoretical models of magnetic field line merging, *Rev. Geophys.*, *13*, 303.

Wygant, J. R., et al. (2005), Cluster observations of an intense normal component of the electric field at a thin reconnecting current sheet in the tail and its role in the shock-like acceleration of the ion fluid into the separatrix region, *J. Geophys. Res.*, *110*, A09206, doi:10.1029/2004JA010708.

F. S. Mozer, Space Sciences Laboratory, University of California, Berkeley, 7 Gauss Way, Berkeley, CA 94720-7450, USA. (fmozer@ssl.berkeley.edu)